LAWRENCE
LIVERMORE
NATIONAL
LABORATORY

LLNL-JRNL-505531

Convergent Pad Polishing

T. I. Suratwala, W. A. Steele, M. D. Feit, R. Desjardin, D. C. Mason

October 13, 2011

International Journal of Applied Glass Science

Disclaimer

This document was prepared as an account of work sponsored by an agency of the United States government. Neither the United States government nor Lawrence Livermore National Security, LLC, nor any of their employees makes any warranty, expressed or implied, or assumes any legal liability or responsibility for the accuracy, completeness, or usefulness of any information, apparatus, product, or process disclosed, or represents that its use would not infringe privately owned rights. Reference herein to any specific commercial product, process, or service by trade name, trademark, manufacturer, or otherwise does not necessarily constitute or imply its endorsement, recommendation, or favoring by the United States government or Lawrence Livermore National Security, LLC. The views and opinions of authors expressed herein do not necessarily state or reflect those of the United States government or Lawrence Livermore National Security, LLC, and shall not be used for advertising or product endorsement purposes.

For Submission to *International Journal of Applied Glass Science*

Convergent Pad Polishing

T. Suratwala, R. Steele, M. Feit, R. Desjardin, D. Mason

[a]*Lawrence Livermore National Laboratory, P.O. Box 808, Livermore, CA 94551, USA*

A new method of optical polishing termed 'Convergent Polishing' is demonstrated where a workpiece, regardless of its initial surface figure, will converge to the shape of the lap in a single iteration. This method of polishing is accomplished by first identifying the phenomena that contribute to non-uniform spatial material removal, quantifying their behavior, and then mitigating the non-uniformity for each phenomenon (except for the workpiece-lap mismatch due to the workpiece surface shape). The surface mismatch at the interface between the workpiece and lap causes a spatial and time varying pressure (and hence removal) differential which decreases with removal (i.e. polishing time), thus allowing the workpiece to converge to the shape of the lap. In the following study, fused silica workpieces (100 mm round & square) are polished using ceria slurry on various polyurethane pads. Polishing parameters were systematically controlled to demonstrate the prevention of various sources of non-uniform material removal which include: 1) moment force, 2) viscoelastic lap relaxation, 3) kinematics, 4) pad wear, and 5) workpiece bending (mechanically or stress induced). The first three are described in detail in our previous study; the latter two are described here. With these mitigations, removal uniformity has been demonstrated to within 1.0 μm over the whole surface after 83 μm of material removal corresponding to a within workpiece non-uniformity (WIWNU) of <1.2%. In addition, convergence has been demonstrated down to 0.18 ±0.04 μm peak-to-valley flatness on 100 mm - sized fused silica workpieces.

1. Introduction

Conventional, full-aperture optical polishing often requires multiple iterative cycles involving polishing, surface figure measurement, and adjustment of polishing parameters to achieve the desired surface figure (i.e., shape). Due to the large number of process variables, the efforts to quantitatively control the shape has been challenging, and hence this process has remained largely artisan-based. Thus, developing a scientific and quantitative understanding of material removal could lead to processes that are more deterministic, allowing optical glass fabrication to be performed in a more repeatable, less iterative, and more economical manner.

At the macroscopic level, material removal has been historically described by the widely used Preston equation [1-2]:

$$\frac{dh}{dt} = k_p \, \sigma_o \, V_r \tag{1}$$

where dh/dt is the average thickness removal rate, σ_o is the applied pressure, and V_r is the average relative velocity of the polishing particle relative to the workpiece. The microscopic and molecular level effects are described macroscopically by the Preston constant (k_p). Many studies, particularly those in the chemical mechanical polishing (CMP) literature for Si wafer polishing which has many similarities to optical finishing, have expanded Preston's model to account for slurry fluid flow and hydrodynamic effects [3-5], Hertzian contact mechanics [6], the influence of asperity microcontact [7-9], and the mechanics of contact on the pressure distribution [10-13]. However, only a few of these studies focus on understanding and predicting surface figure (or global non-uniformity). In such studies, the global surface figure has been described by an analogous term called Within Wafer Non-Uniformity (i.e., WIWNU) which describes the variation in spatial removal across the wafer or workpiece for a given polishing time.

In our previous study [14], material removal and surface figure were measured on fused silica glass that had been polished using cerium oxide slurry on a polyurethane lap under a systematic set of polishing conditions. A spatial and temporal polishing model was formulated and used to simulate the experimental data which incorporated: 1) the friction coefficient as a function of velocity (Stribeck curve), 2) the relative velocity which is determined by the

kinematics of the lap and workpiece motions, and 3) the pressure distribution which is shown to be dominated by: a) moment forces, b) lap viscoelasticity; and c) workpiece-lap interface mismatch. All of these phenomena were represented in a more general form of Preston's Equation described as:

$$\frac{dh_i}{dt}(x,y,t) = k_p \ \mu(v_r(x,y,t))\ \sigma(x,y,z,t)\ \ v_r(x,y,t) \tag{2a}$$

$$\frac{dh}{dt}(x,y,t) = \frac{k_p}{t}\int_0^t \mu(v_r(x,y,t'))\ \sigma(x,y,z,t')\ \ v_r(x,y,t')\ dt' \tag{2b}$$

where dh_i/dt & dh/dt are the instantaneous and time average removal rates, respectively, at some given time t and position (x,y) on the workpiece. μ is the friction coefficient which is a function of the instantaneous relative velocity (v_r) at the workpiece-lap interface. σ is the pressure distribution resulting from the applied pressure (σ_o) and the nature of the workpiece-lap contact.

In addition to the ones described above, two other critical phenomena can influence spatial material removal uniformity: they are: 1) pad wear and 2) workpiece deformation (mechanically or stress induced). Figure 1 schematically illustrates each of these phenomena and its relationship to the material removal rate equation. The influence of pad wear and changes in pad properties during polishing have been previously investigated [15-18]. Here the workpiece and/or conditioner (typically a fixed diamond abrasive to treat the pad for CMP or a sacrificial workpiece used during pad optical polishing) is loaded against the pad surface and, as a result, spatial and temporal changes in the pad properties (thickness profile, roughness, slurry charging level, etc.) can occur. Since the size of the workpiece and/or conditioner is typically not the same size as the lap and since the kinematic controls are largely focused on achieving uniform removal on the workpiece, the pad usually sacrificially wears non-uniformly, resulting in a workpiece-lap mismatch, a non-uniform pressure distribution, and non-uniform material removal [14]. Chang et. al. [16] modeled the typical kinematics of the conditioner and showed that the conditioner will wear the pad non-uniformly resulting in a concave pad surface. Park et. al. [18] showed that the wafer (or workpiece) also contributes to non-uniform pad roughness and thickness of a polyurethane foam pad. In the following study, the wear rate of the pad is quantified, the Preston model is expanded to simultaneously account for pad wear and workpiece material removal, and a new method to counteract non-uniform pad wear is demonstrated.

Mechanical bending of or residual stress in a high-aspect-ratio (i.e., diameter/thickness) workpiece or lap can also contribute to a change in the workpiece-lap mismatch. Depending on the type of removal desired, workpiece bending can be a desired or an undesired feature. For example, when polishing Si wafers during CMP, uniform removal over the whole workpiece is desired. Ng et. al. [19] measured the degree of silicon wafer bending during CMP and compared it to finite element analysis calculations. Workpiece bending is typically aided by using a compliant sub-pad which reduces the workpiece-lap mismatch and results in improved WIWNU. However, in the case of optical finishing where the workpiece is initially not at the desired surface figure, workpiece bending would be undesirable because it would interfere with the workpiece converging to the shape of the lap.

In any optical fabrication process, there is a transition from grinding (removal by fracture) to polishing (removal by chemical means). During polishing, the removal of the ground surface layer of the workpiece, which is known to be in high compression [20], changes the equilibrium stress field in the workpiece. An unconstrained workpiece ground on one face will bend, changing the surface figure (referred to as the Twyman effect [21,22]). Lambropoulos et. al. [23] quantified the Twyman stress for a variety of grinding processes, where the magnitude of the stress scaled with the abrasive size used during grinding. A similar study was performed by Chen et. al. [24] on Si wafers. In the following study, the influence of mechanical bending and residual stress on the workpiece-lap mismatch and material removal uniformity is measured, and methods to control these effects are explored.

Lastly, in this study, we introduce an alternative and novel method for polishing, called ‘Convergent Polishing’. With this method, each of the sources of the workpiece non-uniform material removal (discussed above) is mitigated in some manner except for the workpiece-lap mismatch due to the workpiece shape. For counteracting pad wear, a uniquely-shaped glass septum is used; for preventing workpiece deformation effects, pitch button blocking and chemical etching techniques are used. Using these combined techniques, Convergent Polishing is demonstrated where a workpiece, regardless of its initial shape, will converge to the desired surface figure without requiring changes to the polishing parameters and without the need for multiple polishing iterations.

2. Experimental

Round and square silica glass samples (Corning 7980; 100 mm in diameter or diagonal x 2.2-10 mm thick; initially polished by Sydor Optics) were re-polished on an orbital polisher under various conditions as described in Table 1. A few of the samples were initially re-ground using alumina abrasives (Microgrit 9T or 30T) by hand grinding (5 min, random kinematics, cast iron lap, 2068 Pa (0.3 psi) pressure). Re-polishing was performed on various polyurethane pads (SUBA 550 with square patterned grooves (2 mm width with 10 mm spacings) or IC1000 with standard k-grooves) adhered to an aluminum or granite base plate (300 mm in diameter x 50 mm thick). The pads were preconditioned using a CMP diamond conditioner (Diamonex 250355FT) in the presence of water or ceria slurry. The workpiece was uniformly loaded at 2068 Pa using a steel weight attached by double sided tape, by pitch button blocking (Blocking Pitch-1 Black, Universal Photonics, 11 buttons, 4.5 mm diameter, heated to 60^{o}C and isothermally cooled at ~6^{o}C/hr), or by foam blocking (3 mm thick poster tape). The workpiece was rotated using a motor driven guide wheel at the trailing edge of the workpiece. Cerium oxide slurry (Hastilite PO, Universal Photonics, ~0.4 μm mean particle size; diluted to Baume 9 with water) was magnetically stirred externally and distributed onto the lap using a peristaltic pump (Masterflex L/S) at a flow rate of 0.6 ml/minute. The kinematic parameters on the orbital polisher include the rotation rate of the lap (R_L), rotation rate of the workpiece (R_o), separation distance between the workpiece center and lap center (s), stroke rate (R_s), and stroke distance (d_s). All samples were polished using the same kinematics (R_L=20 rpm, R_o=20 rpm, s=75 mm, R_s=3 rpm, d_s=0.5 cm). In certain experiments, a pad wear compensating septum of various designs was used as noted in Table 1. A borosilicate glass sheet (1.1. mm thick) with the same shape as the septum was adhered by foam tape to the septum weight; the resulting uniform applied pressure on the septum glass was 2068 Pa (0.3 psi). Figure 2 shows photos of the polishing setup for samples that were polished with a septum. The weight of the workpiece (±0.001 gms) and the reflected wavefront of the polished face of the workpiece (using a Michelson Interferometer, 4" ADI Phaseshift MiniFiz 100) were measured after each polishing iteration.

The pad wear rate, and hence the pad's Preston coefficient, was measured using an experimental setup shown schematically in Figure 3. Three square fused silica coupons (1 x 1 x 0.5 cm^3), loaded at a uniform pressure of 2068 Pa (0.3 psi) using steel weights, were polished at various distances (s) from the lap center. After each polishing iteration, a thin radial slice of the pad was removed and its cross sectional thickness was measured (using optical microscopy). The change in pad thickness with polishing time was used to determine the pad's Preston constant.

3. Results

Figure 4 shows the results of the measured pad wear rate of the Suba 550 polishing pad for the experiment described in Figure 3. The wear rate was initially high but decreased with polishing time and then stabilized, suggesting a large change in pad properties with polishing for a new pad. From the data, the lap Preston constant (k_{lap}) can be empirically described as a single exponential decay as a function of time (t) in the form:

$$k_{lap}(t) = k_{o\,lap} e^{-t/t_{lap}} \tag{3}$$

where k_{olap}=1.65x10^{-4} μm m/N and t_{lap}=23 hr. Note the initial value of Pad's Preston constant is ~100 greater than the Preston constant for the fused silica workpiece (k_p=1.9 x10^{-6} μm m/N) [14]. However, the aged lap shows wear that is equivalent or less than that of the workpiece.

Table 1 summarizes the fused silica workpiece polishing experiments showing both the initial and final Peak-to-Valley (PV_q) of the full aperture surface from the reflected wavefront interferometry measurements, as well as the major process variables (i.e., workpiece shape, workpiece thickness, initial surface shape & treatment, pad type, septum type, and mounting conditions). Note PV_q is reported as the maximum height difference on the measured surface after 1% of the low and high data points have been discounted to minimize sensitivity due to anomalous data points. Positive PV_q values describe concave surfaces, and negative values describe convex surfaces. The average removal rate on the workpiece for each of the polishing experiments ranged from 0.7-1.0 μm/hr.

The polishing configuration strongly influenced the final PV_q and uniformity of the removal. Figure 5 illustrates this by plotting the PV_q of the initially flat workpieces as a function of polishing time for various polishing conditions. Using the appropriate configuration, it is possible to achieve uniform removal as illustrated by Sample H1. Figure 6 shows the lineouts of the surface figure of three selected samples from Figure 5 as a function of polishing time. Figures 7a-d plot the PV_q as a function of polishing time for workpieces with different initial surface figures for four different configurations demonstrating Convergent Polishing. Figures 8-9 shows the 3D surface profile evolution of

selected samples from Figure 7. Note the surface shapes are all plotted on a single color scale for a given polishing run (as noted in the figure caption).

Figure 10 shows the 3D surface figures before and after polishing using either foam (compliant) blocking or pitch (stiff) button blocking on high aspect ratio (AR) workpieces (100 mm x 2.2 mm thick; AR=45). The results suggest that uniform spatial removal is largely achieved using foam blocking despite a non-flat initial workpiece surface (due to workpiece bending) while non-uniform removal is achieved (due to workpiece–lap mismatch) using pitch button blocking leading to convergence to the shape of the lap.

Figures 11a-d show the 3D surface figures before and after grinding with 9 μm or 30 μm loose abrasive of the opposing surface of high aspect ratio (AR) workpieces (100 mm x 2.2 mm thick; AR=45). The results show that grinding leads to significant stress causing in deflection of the workpiece which can be observed on the opposing surface. In Figure 11e, it is shown that by chemically etching the ground surface, the surface figure can be largely returned to its initial state by removing the stress layer. Figure 12 also shows the removal of the stress layer with polishing through the observation of a decreasing PV_q of the opposing surface with incremental polishing of the ground surface.

4. Discussion

4.1 Pad wear

As discussed above, pad wear can evolve temporally and spatially in a complex way. One can describe the time average pad wear in a similar manner as material removal from the workpiece with a Preston type equation in the form of:

$$\frac{dh_{lap}}{dt}(x,y,t) = \frac{f_o(r)}{t} \int_0^t k_{lap}(t')\,\mu(x,y,t')\,v_r(x,y,t')\,\sigma(x,y,z,t')dt' \tag{4}$$

where $f_o(r)$ is the fraction of the lap circumference loaded by the workpiece as a function of radial distance (r) from lap center and k_{lap} is the lap Preston constant. μ, v_r and σ are synonymous to that shown in Eq. 2. For a round workpiece, $f_o(r)$ can be described as:

$$f_o(r) = \frac{\theta_L(r)}{2\pi} = \frac{\arcsin\left(\frac{x_L(r)}{r}\right)}{\pi} \tag{5}$$

where θ_L is the solid angle of the lap covered by the workpiece, and $x_L(r)$ is the x component of a point on the leading edge of the workpiece (see Figure 13 for schematic). Using the geometry relations of:

$$x_L^{\,2} + y_L^{\,2} = r^2 \tag{6a}$$

$$x_L^{\,2} + (y_L + s)^2 = r_o^{\,2} \tag{6b}$$

results in:

$$x_L(r) = \sqrt{-\left(\frac{r_o^{\,2} - s^2 - r^2}{2s}\right)^2 + r^2}\,. \tag{7}$$

With a uniform pressure loading and matched rotation (R_o=R_L), k_{lap}, μ, σ, and v_r are spatially constant, and hence the non-uniformity of the lap wear due to the workpiece is dominated by $f_o(r)$. In this case, the pad wear rate (Eq. 4) simplifies to:

$$\frac{dh_{lap}(r)}{dt} = 2\arcsin\left(\frac{x(r)}{r}\right) k_{lap}\ \mu\ R_o\ s\ \sigma_o \tag{8}$$

where the time average relative velocity is $V_{ro}=2\pi R_o s$. Note that even though k_{lap} can be nonlinear with time, it does not vary spatially. Using Eq. 8 for typical polishing conditions, the calculated pad wear rate spatial profile is shown in Figure 14a. The calculated profile is qualitatively consistent to the pad profile measured experimentally by Park et. al. [18] after polishing many Si wafers under similar kinematic conditions. Because pad wear is greatest near the workpiece center, the surface figure of the workpiece is expected to become convex due to the greater workpiece-lap mismatch and pressure drop in the center versus the edges of the workpiece. In this study, we also observe the workpiece taking a convex shape as shown in Figures 6a&b with long time polishing without a septum. On a new Suba 550 pad, the rate of turning convex is higher due to the large lap Preston coefficient (see Eq. 3). In both cases (new or used pads), the WIWNU has high values of 92% and 27%, respectively.

To date, several methods have been used to reduce the impact of pad wear including kinematically-controlled diamond conditioning and altering workpiece kinematics [25]. However, kinematically-controlled diamond conditioning, where the diamond conditioner strokes back and forth across pad, can dramatically reduce pad lifetime and the kinematics are difficult to optimize for spatially uniform pad wear. Also, workpiece kinematic control is challenging because it is very difficult to optimize both workpiece and pad wear uniformity simultaneously. Hence an alternative method is proposed here where a glass septum (i.e., a sacrificial workpiece that also results in wear on the pad) is used to counteract the pad wear spatial non-uniformity caused by the workpiece [26]. To design such a septum, the basic criterion is that the total rate of radial pad wear due to both the workpiece and septum is kept constant (see Figure 14a):

$$\frac{d\,h_{lap}(r)}{dt} = C = f_o(r)\,k_{lap}\,\mu\,V_{r\,o}\sigma_o + f_s(r)\,k_{lap}\,\mu\,V_{r\,s}\sigma_s \tag{9}$$

where $f_s(r)$ is the fraction of the lap circumference loaded by the septum as a function of radial distance (r) from the lap center, C is a chosen constant for the removal rate on the pad, V_{rs} is the time average relative velocity on the septum which is given by $2\pi R_L r$, and σ_s is the applied pressure on the septum. For conditions of matched rotation ($R_L=R_o$) and matched workpiece & septum pressures ($\sigma_o=\sigma_s$), the septum shape can be determined from:

$$f_s(r) = \frac{C}{2\pi\,k_{lap}\,\mu R_o\,r\,\sigma_o} - \arcsin\left(\frac{x_L(r)}{r}\right)\frac{s}{\pi\,r}\,. \tag{10}$$

Using Eq. 10, the calculated radial width of the septum ($2\pi r f_s(r)$) is shown in Figure 14b. Note that there are two limits in the design of the septum as designated by the dashed lines in Fig. 14b. The first one is the minimum radial width of the septum which is needed for structural integrity and to allow a minimum distance for pad viscoelastic relaxation (see ref [14] for details). The second is a limit near the lap center where the circumference of the pad needs to be large enough to provide the required counter wear by the septum. The latter limit can be expanded by applying a higher load on the septum and/or by increasing the separation distance **s** between the lap and workpiece center. Figure 2 shows photos of two septums (one for round workpiece and another for square workpiece) within the polishing setup used in this study. Note Eq. 10 applies only for a round workpiece, and the septum design for a square workpiece was determined numerically using Eq. 9. The effectiveness of the septum in reducing pad wear, as measured by uniformity in removal on the workpiece, is illustrated by comparing Sample H1 with G1 & G2 in

Figures 5& 6. Using the septum, the WIWNU uniformity was significantly reduced to <1.2% with Sample H1. In other words, only ~1 μm deviation was observed after polishing 83 μm of material from the surface.

4.2 Mechanical Workpiece Bending

As discussed in the introduction, an important phenomenon affecting workpiece-lap mismatch and removal uniformity is workpiece bending. The amount that a workpiece will bend during polishing depends on many factors including: workpiece geometry (e.g., shape, AR), material properties (e.g., elastic modulus), initial surface figure, and mounting conditions. To quantify the effect of AR on bending, finite element analysis (using ProEngineer ProMechanica) was performed on a fused silica workpiece (150 mm diameter) with varying thicknesses. The workpiece, initially with a concave surface (PV_q=15.8 μm), was simply supported at the edges and a uniform pressure (σ_o=2068 Pa or 0.3 psi) was applied. The results, shown in Fig. 15, indicate that a thick workpiece (t_o=10 mm or AR<15) will not bend significantly, whereas a thin workpiece (t_o<3.3 mm or AR>45) will bend significantly. Insight to the amount a workpiece will bend can also be determined analytically by calculating the amount that a simply supported flat, uniform thickness plate (i.e., workpiece) would bend under uniform pressure (σ_o) (without the presence of a lap), which is given by:

$$z_{\max} = 0.695\,\sigma_o \frac{(2r_o)^4}{E_o\, t_o^{\,3}} \tag{11}$$

where r_o is the workpiece radius, E_o is the workpiece elastic modulus, and t_o is the workpiece thickness [27]. Note that z_{max} is proportional to ~AR^3 which suggests that degree of deflection is strongly dependent on the AR of the workpiece.

The method of mounting can be used as a means to control the amount of workpiece bending during polishing. In cases where workpiece bending is desired, a compliant interface between the workpiece and loading weight can be used such as foam (i.e., having a low elastic modulus). Figures 10a-b show the results of polishing a concave surface on a high AR workpiece, which remains largely concave after polishing due to the compliant mounting. The bending

of the workpiece allows for minimizing the workpiece-lap mismatch and for minimizing the spatial variation in the pressure distribution. This results in uniform removal on the workpiece and no change in the workpiece shape.

Achieving a mounting condition for a high AR workpiece that prevents workpiece bending is more challenging. One can mount to a stiff mounting block; however, the degree of workpiece bending will be dependent on both the opposing surface of the workpiece (side not being polished) and the shape of the surface of the mounting block. To reduce this dependency, an optical fabrication technique referred to as 'pitch button blocking' can be used [28]. This mounting technique uses small islands of pitch between the workpiece and the mount which are cooled from the softening temperature of the pitch. At room temperature, the workpiece-pitch button-mount system is stiff, and the workpiece largely maintains its initial surface figure. Figures 10c-d show the results of polishing a concave surface on a high AR workpiece using pitch button blocking. After polishing, the workpiece converged to the shape of the lap because of the lack of workpiece bending and a dominance of the workpiece-lap mismatch due to the workpiece shape effect on the pressure distribution.

4.3 Grinding Stress Workpiece Bending

Another mechanism by which workpiece bending can occur is due to the residual compressive stress left behind on the workpiece during grinding [20,21] (see discussion in Introduction). To confirm this effect, samples were ground on one side of a polished workpiece, and the change in the surface figure of the opposing surface was measured. Figures 11a-d show the results after grinding with 9 μm & 30 μm alumina, which caused the opposing surface to deform significantly (3.51 μm and 6.5 μm concave, respectively). The magnitude of the stress can be inferred from the following form of the Twyman stress equation [29] given by:

$$PV_q = \frac{3}{4}\frac{P_c(1-\nu)}{E_o}\left(\frac{2r_o}{t_o}\right)^2 \tag{12}$$

where P_c is the Twyman stress and ν is the workpiece Poisson's ratio. Based on these deflections, P_c= 270 N/m using 9 μm alumina and P_c=420 N/m using 30 μm alumina. These values match well and scale similarly with particle size to those reported by Lambropoulos et. al. [23] and Podzimek et. al. [30].

The residual stress on the ground workpiece will be additive to the applied load during polishing. Hence, residual stress can influence workpiece bending, and hence the workpiece-lap mismatch and removal uniformity. However, since a ground surface cannot be measured interferometrically, it is difficult to quantify this effect. Instead, we explore two methods to remove the residual stress: 1) by polishing away the ground surface during a separate process step or 2) by chemically etching the surface to remove the residual stress. The results for incrementally polishing a ground surface and its impact on the final workpiece shape (of opposing surface) are shown in Figure 12. As polishing occurs, the residual stress layer is incrementally removed, and the resulting Twyman stress induced surface figure change is reduced. From the results in Figure 12, the depth of the residual stress layer is <10 μm. Hence, by pre-polishing away at least 10 μm, one can remove the residual stress and avoid potential effects on removal uniformity. Alternatively, one can etch the ground surface using, for example, NH_4F:HF. After removing ~10 μm of material by etching, the surface figure of the opposing surface returns nearly to its pre-ground state (see Fig. 11e), confirming the ability to remove the residual stress and its potential effects on removal uniformity. Note that etching a ground surface has other advantages such as exposing scratches for surface quality assessment and reducing the amount of material removal needed to polish through the sub-surface mechanical damage from the grinding process [30-31].

4.4 Convergent Polishing

With a systematic understanding of the key phenomena affecting material removal (see Figure 1) and their contribution to spatial non-uniform removal as described in this study and in an earlier work [14], methods to achieve the goal of full aperture deterministic optical polishing can now be addressed. One method is to polish and incorporate all of the phenomena described above quantitatively into a code, such as our SurF program [14], and calculate the optimum polishing parameters to get to the desired surface figure. However, this technique for deterministic finishing is challenging due to the large number of process variables which leads to difficulty in calculating a minima in the solution. Another method for achieving deterministic finishing is to remove all the sources of non-uniformities in material removal on the workpiece (through engineering and polishing process parameters controls) except for the workpiece shape induced workpiece-lap mismatch. The surface mismatch at the interface between the workpiece and lap causes a spatial and time varying pressure (and hence removal) differential which decreases with removal (i.e. polishing time) [14], thus allowing the workpiece to converge to the shape of the lap. This technique, named Convergent Polishing [26], would allow for polishing workpieces (flat or spheres) in a single iteration using a single set of polishing parameters regardless of the initial shape of the workpiece and without the need for initial and during-process surface figure metrology.

Table 2 delineates the same phenomena illustrated in Figure 1 along with proposed methods to prevent the non-uniform removal. Using these controls, Convergent Polishing has now been demonstrated (see Figure 7) for: (a) low AR round workpieces on a Suba 550 pad, (b) low AR round workpieces on IC1000, (c) low AR square workpieces on IC1000, and (d) high AR round (ground or polished) workpieces on IC1000. In all of these polishing runs, the workpieces with varying initial surface figures were polished identically, and they all converged to a final, nominally flat shape. We believe this is the first demonstration of convergent full aperture polishing. Figures 8 & 9 illustrate the 3D surface figure convergence with polishing time for the round and square parts. In Figure 8, simulations using the SurF code show good agreement with experimental data. Details of the SurF algorithm are described elsewhere [14]. Note that the simulation incorporates all the phenomena listed in Table 2 (except for temperature effects) and the corresponding mitigations including use of a septum. Also, the simulation uses no fitting parameters, only known material properties and parameters determined from previous polishing runs (e.g. Preston constant (k_p), gap constant ($\bar{h}$), and workpiece slope (θ_x)) [14].

The convergence point varied with each polishing configuration in Figure 7 ranging from 0.18-1.0 μm. The control of the convergence point is the next area of study, which likely involves a more detailed understanding of other phenomena such as: 1) effect of slurry temperature, 2) long term stability of pad material properties, 3) effect of diamond conditioning, and 4) the initial shape of the pad. To date, convergence point control has been demonstrated as low as 0.18 ±0.05 μm on a 100 mm workpiece.

5. Summary

The evolution of the surface figure of various fused silica workpieces (round & square; low & high AR; ground vs polished) was measured after polishing under a systematic set of polishing parameters to understand sources on the spatial non-uniform removal due to a workpiece-lap mismatch (including workpiece shape, pad wear, workpiece bending, and residual stress). To prevent non-uniform pad wear, a specifically shaped septum was designed and used. To prevent workpiece bending during polishing on high AR workpieces, mounting techniques such as pitch button blocking were shown to be effective. Finally, to prevent residual stress effects from previous grinding processes, pre-polishing and chemical etching methods were demonstrated. Applying these methods and others (proposed in our previous study [14]) to prevent non-uniform material removal, a new method of polishing, Convergent Polishing, is demonstrated. In this method, the workpiece, regardless of its initial surface figure, can be polished to the shape of the lap in a single polishing iteration using a single set of polishing parameters and without the need for initial and in-process surface figure metrology.

Acknowledgements

This work performed under the auspices of the U.S. Department of Energy by Lawrence Livermore National Laboratory under Contract DE-AC52-07NA27344. The authors would like to also acknowledge the useful conversations with R. Dylla-Spears, L. Wong, P. Miller, and J. Bude, and engineering support from P. Harriss, E. Northcutt, J. Bigelow, P. Geraghty, and D. Fisher.

Table 1. Summary of polishing experiments.

Series	Exp	Workpiece Shape	Workpiece Thickness (mm)	Initial surface quality	Pad	Septum Type	Mounting[1]	PV_q Initial (μm)	PV_q Final (μm)
Towards Uniform Removal	G1	Round	10	Polished	Suba 550[2]	none	taped	0.35	6.06
	G2	Round	10	Polished	Suba 550	none	taped	0.16	4.24
	G3	Round	10	Polished	IC1000	none	taped	0.21	4.78
	G4	Round	10	Polished	Suba 550	R*	taped	0.32	2.51
Round Workpiece on Suba	H1	Round	10	Polished	Suba 550	R	taped	-0.20	-1.04
	H2	Round	10	Polished	Suba 550	R	taped	-0.91	-1.1
	H3	Round	10	Polished	Suba 550	R	taped	6.50	-0.95
	H4	Round	10	Polished	Suba 550	R	taped	-7.00	-1.95
Round Workpiece on IC1000	I1	Round	10	Polished	IC1000	R	taped	-0.28	-0.49
	I2	Round	10	Polished	IC1000	R	taped	-4.76	0.43
	I3	Round	10	Polished	IC1000	R	taped	9.90	0.32
Square Workpiece on IC1000	J1	Square	10	Polished	IC1000	S	taped	0.24	0.22
	J2	Square	10	Polished	IC1000	S	taped	5.40	0.19
	J3	Square	10	Polished	IC1000	S	taped	-7.00	0.13
High Aspect Ratio Workpiece	K1	Round	2.2	Polished	IC1000	R	PBB[4]	49.00	0.31
	K2	Round	2.2	Polished	IC1000	R	FB[5]	13.8	12.3
	K3	Round	2.2	9T	IC1000	R	PBB	3.68	0.41
	K4	Round	2.2	30T	IC1000	R	PBB	7.70	-1.35
	K5	Round	2.2	9T+etch[3]	IC1000	R	PBB	0.25	0.51

[1]Mounting=interface between loading weight and top surface of workpiece; [2]New Suba 550 pad (other samples were polished on a pad after 100 hrs of pre-polish); [3]Sample on top side was ground with 9T microgrit followed by HF/NH_4F etching; [4]PBB=Pitch Button Blocking; [5]FB=Foam Blocking. Septum R and S are the designed septums for round and square workpieces, respectively, as shown in Figure 2. Septum R* is the same as Septum R except located ~10 cm from the leading edge of workpiece.

Table 2: List of polishing parameters affecting non-uniform material removal and methods for preventing non-uniformity.

Parameter			Affects non-uniform removal?	Methods for preventing removal non-uniformity
1. Preston Constant (temperature dependence)			Yes	1) Implement Slurry temperature control; 2) Use septum to minimize temperature non-uniformity on pad; 3) Improve slurry heat distribution by groove design; 4) Reduced time average velocity to minimize friction induced
2. Friction Coefficient			No	NA
3. Relative Velocity (Kinematics)			Yes	Use kinematics with constant spatial time average relative velocity (e.g., $R_O=R_L$; $d_s=0$)
4. Pressure Distribution	4.1 Applied Load Distribution		Yes	Use uniform loading
	4.2 Elastic Lap Response		Yes	Use retaining ring [14]
	4.3 Hydrodynamic Forces		Yes	Operate with total applied load high enough to be in Contact mode (i.e., no hydrodynamic effect) [14]
	4.4 Moment Force		Yes	Minimize moment arm using side wheel optic rotation and mount without a pivot point [14]
	4.5 Viscoelastic		Yes	Use septum to pre-strain lap at leading edge of optic [14]
	4.6 Workpiece-Lap Mismatch	4.6.1 Workpiece Shape	Yes	Do not mitigate; use as the control for achieving Convergent Polishing
		4.6.2 Pad Wear	Yes	Use appropriate septum geometry to ensure uniform pad wear
		4.6.3 Workpiece Bending	Yes	1) Stiffen lap and optic to minimize deformation (e.g., use thick lap or workpiece); 2) Use pitch button blocking to mount high aspect ratio workpiece
		4.6.4 Residual Grinding Stress	Yes	1) Pre-polish away stress layer; 2) Etch workpiece to remove residual stress on ground surfaces
		4.6.5 Temperature	Yes	Same mitigations as listed in 1

6. References

[1] N. J. Brown, "A short course in optical fabrication technology", Optical Society of America Annual Meeting (1981), LLNL Preprint, UCRL-86796.

[2] F. Preston, "The structure of abraded glass surfaces", *Trans Opt. Soc.* **23 (3)** 141 (1922).

[3] E. Terrell, C. Higgs, "Hydrodynamics of slurry flow in chemical mechanical polishing", *J. Electrochem. Soc.* **153 (6)** K15-22 (2006).

[4] S. Runnels, L. Eyman, "Tribology Analysis of Chemical Mechanical Polishing", *J. Electrochem. Soc.* **141 (6)** 1698 (1994).

[5] S. Park, C. Cho, Y. Ahn, "Hydrodynamic analysis of chemical mechanical polishing process", *J. Tribology International* **33** 723-730 (2000).

[6] L. Cook, "Chemical processes in glass polishing", Journal of Non-Crystalline Solids **120** 152-171 (1990).

[7] Y. Jeng, P. Huang, W. Pan, "Tribological Analysis of CMP with partial asperity contact", *J. Electrochem. Soc.* **150 (10)** G630-637 (2003).

[8] Y. Jeng, P. Huang, "Impact of abrasive particles on the material removal rate", *Electrochem. Solid-State Lett.* **7 (2)** G40-43 (2004).

[9] J. Lu, D. Dornfeld, "Material removal mechanism in chemical mechanical polishing", *IEEE Trans. Semicond. Manuf.* **14 (2)** 112 (2001).

[10] S. Sivaram, H. Bath, E. Lee, R. Leggett, and R. Tolles, "Measurement and modeling of pattern sensitivity during chemical-mechanical polishing of interlevel dielectrics," SEMATECH, Austin, TX, Tech. Rep., 1992.

[11] D. Wang, J. Lee, K. Holland, T. Bibby, S. Beaudoin, and T. Calea, "Von Mises Stress in Chemical Mechanical Polishing Process" *J. Electrochem. Soc.***144 (3)** 1191 (1997).

[12] T.-K. Yu, C. C. Yu, and M. Orlowski, "A statistical polishing pad modelfor chemical mechanical polishing," *IEDM Tech. Dig.* 1993.

[13] Y. Li, "Microelectronic Applications of Chemical Mechanical Planarization", John Wiley & Sons (2007).

[14] T. Suratwala, M. Feit, R. Steele, "Material removal and surface figure during pad polishing of fused silica", *J. Am. Ceram. Soc.* **93(5)** 1326-1340 (2010).

[15] C. Chen, C. Yu, S. Shen, M. Ho, "Operational aspect of chemical mechanical polishing," *J. Electrochem. Soc.* **147 (10)** 3922-3930 (2000).

[16] O. Chang, H. Kim, K. Park, B. Park, H. Seo, H. Jeong, "Mathematical modeling of CMP conditioning process", *Microelectron. Eng.* **84** 577–583 (2007).

[17] Y. Zhou, E. Davis, *Mat. Sci. Eng. B.* **68** 91–98 (1999).

[18] B. Park, H. Lee, K. Parka, H. Kimb, H. Jeong, "Pad roughness variation and its effect on material removal profile in ceria-based CMP slurry," *J. Mater. Process. Technol.* **203** 287-292 (2008).

[19] S. Ng, I. Yoon, C. Higgs III, S. Danyluk, "Wafer-Bending Measurements in CMP," *J. Electrochem. Soc.* **151 (12)** G819-G823 (2004).

[20] A. J. Dalladay, "Some measurements of the stresses produced at the surfaces of glass by grinding with loose abrasives," *Trans. Opt. Soc. London* **23** 170–173 (1922).

[21] F. Twyman, "Polishing of glass surfaces," *Proceedings of the Optical Convention*, Northgate & Williams, London 78 (1905).

[22] F. Twyman, *Prism and Lens Making,* Hilger & Watts, London, **Ch.9** 318 (1952).

[23] J. Lambropoulos, S. Xu, T. Fang, and D. Golini, "Twyman effect mechanics in grinding and microgrinding," *Appl. Opt.* **35 (28)** 5704-5713 (1996).

[24] J. Chen, I. DeWolf, "Study of damage and stress induced by backgrinding in Si wafers," *Semicond. Sci. Technol.* **18** 261–268 (2003).

[25] H. Liang, D. Craven, *Tribology in Chemical-Mechanical Planarization,* CRC Press (2005).

[26] T. Suratwala, R. Steele, M. Feit, R. Desjardin, D. Mason, R. Dylla-Spears, L. Wong, P. Miller, P. Geraghty, "Method and System of Convergent Polishing", U.S. Patent Provisional Application 61454893 March 21, 2011.

[27] R. Roark, W. Young, *Formulas for Stress and Strain*, 5th Ed, McGraw-Hill (1982) 382.

[28] R. DesJardin, "Automated Pitch Button Dispensing Station and Method" US Patent 6692573 (Feb 17 2004).

[29] W. J. Rupp, "Twyman effect for ULE," in *Optical Fabrication and Testing Workshop* Optical Society of America, Washington, D.C. 25–30 (1987).

[30] O. Podzimek, “Residual stress and deformation energy under ground surfaces of brittle solids,” *Ann. CIRP* 35 397-400 (1986).

[31] L. Wong, T. Suratwala, M. D. Feit, R. Steele, "The Effect of HF/NH_4F Etching on the Morphology of Surface Fractures on Fused Silica", *J. Non-Crystal. Solids* **355** 797 (2009).

[32] T. Suratwala, L. Wong, P. Miller, M. Feit, J. Menapace, R. Steele, P. Davis, D. Walmer, "Sub-surface mechanical damage distributions during grinding of fused silica," *J. Non-Crystal. Solids* **352** 5601 (2006).

Figure Captions

Figure 1. Schematic illustration of the expanded Preston Equation (Eq. 2) describing the phenomena that effect spatial and temporal material removal during polishing.

Figure 2. Photos of the convergent polishing setups for (a) round and (b) square workpieces with accompanying pad-wear compensating septums.

Figure 3. Schematic of setup to measure pad wear.

Figure 4. Measured pad removal rate due to polishing fused silica coupons as described in the setup in Fig. 3. The lines are single exponential fits to the measured data.

Figure 5. Change in polished surface Peak-to-Valley height (PV_q) as a function of polishing time for various polishing conditions. All samples started nominally flat (PV_q<0.5 μm). Samples E1 and D5 are data from [14].

Figure 6. Radial surface profile of fused silica workpieces using (a) a new (Sample G1) and (b) an aged (Sample G2) Suba 550 polishing pad after each polishing iteration. (c) Radial surface profile of the fused silica workpiece after each polishing iteration for Sample H1 in which sources of non-uniformity have been mitigated (as listed in Table 2).

Figure 7. Convergent polishing demonstration on a variety of workpiece types and pads: (a) round workpiece (100 x 10 mm) on a Suba 550 pad; (b) round workpiece (100 mm x 10 mm) on IC1000; (c) square workpiece (100 mm diagnol x 10 mm) on IC1000; and (d) round, high AR workpiece (100 mm x 2.2 mm) on IC1000. Lines in (b) and (c) are SurF simulation results as described in Section 4.4.

Figure 8. Surface figure of a round workpieces as a function of polishing time illustrating convergence for (a) an initially concave workpiece (Sample I3) (full scale -6.5 μm to 5.5 μm) and for (b) an initially convex workpiece (Sample I2) (full scale -3.0 μm to 3.0 μm). The top row represents the measured data and the second row is the simulation results using SurF Code.

Figure 9. Surface figure of a square workpiece as a function of polishing time illustrating convergence for an initially concave workpiece (Sample J2) (full scale -3.0 μm to 5.5 μm) **(top)** and an initially convex workpiece (Sample J3) (full scale -6.0 μm to 3.0 μm) **(Bottom)**.

Figure 10. Surface figure of a high AR workpiece (100 mm x 2.2 mm thick) using foam (compliant) blocking (Sample K1) (a) before and (b) after polishing (full scale -8.0 μm to 6.0 μm). Surface figure of a high AR workpiece (100 mm x 2.2 mm thick) using pitch (stiff) button blocking (Sample K2) (c) before and (d) after polishing (full scale -18 to 5 μm).

Figure 11. Surface figure of a high AR workpiece (100 mm x 2.2 mm thick) (a) before and (b) after grinding the opposing surface with 9 μm alumina abrasive (Sample K3). Surface figure of a high AR workpiece (100 mm x 2.2 mm thick) (c) before and (d) after grinding the opposing surface with 30 μm alumina abrasive (Sample K4). (e) Surface figure of sample K3 shown in (b) after etching in NH_4F:HF for 30 min. All surface figures are plotted at same full scale -3.5 to 3.5 μm.

Figure 12. Surface figure of the opposing surface in terms of PV_q of high AR workpieces (100 mm x 2.2 mm thick) initially ground with 9 μm or 30 μm alumina abrasive and then subsequently polished for various times.

Figure 13. Schematic of the polishing setup illustrating the coordinate system and geometry associated with a point (x_L,y_L) at the leading edge of the workpiece and its corresponding path on the lap.

Figure 14. (a) Calculated pad wear rate using Eq. 8 for round workpiece polishing conditions used in this study (μ=0.7, σ_o=2068 Pa (0.3 psi), R_o=20 rpm, s= 75 mm, r_o=50 mm, r_{lap}=150 mm); (b) Calculated septum radial width for a round workpiece using Eq. 10.

Figure 15. Calculated surface profile of fused silica workpieces (r_o=150 mm, initial PV_q=15.8 μm) with different thicknesses (t_o) or aspect ratios (AR) after being loaded at 0.3 psi. The solid line is the free standing initial surface profile; the dashed lines are the resulting surface profile under applied load.

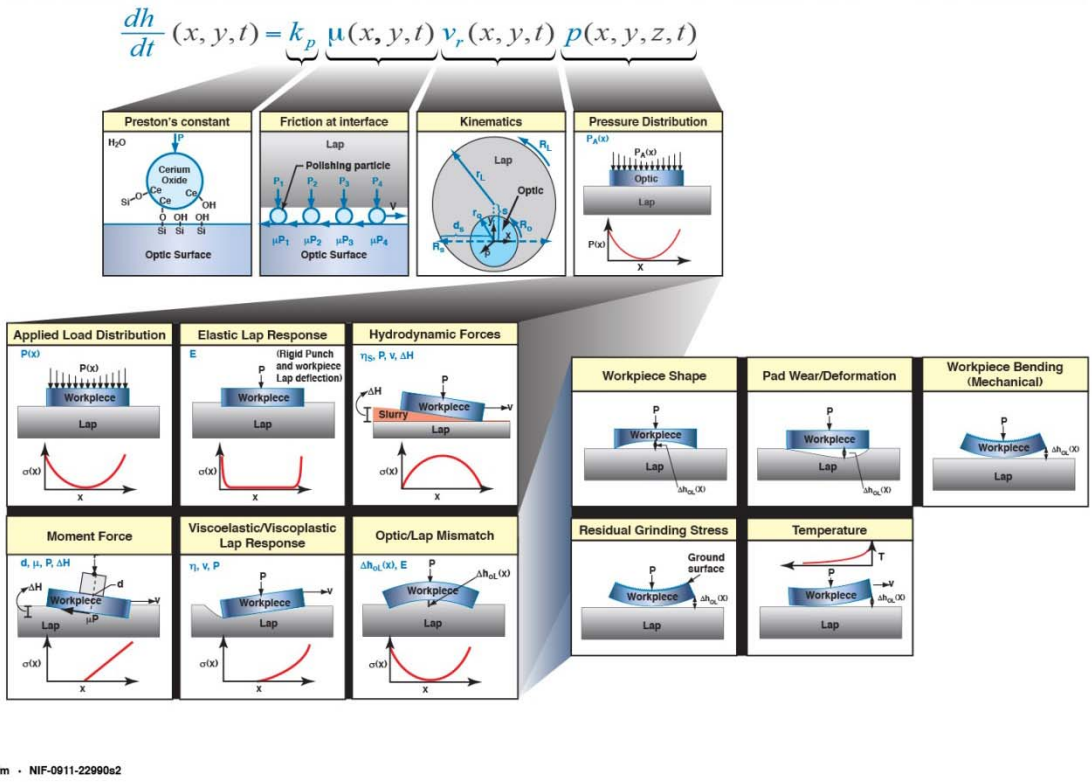

Figure 1.

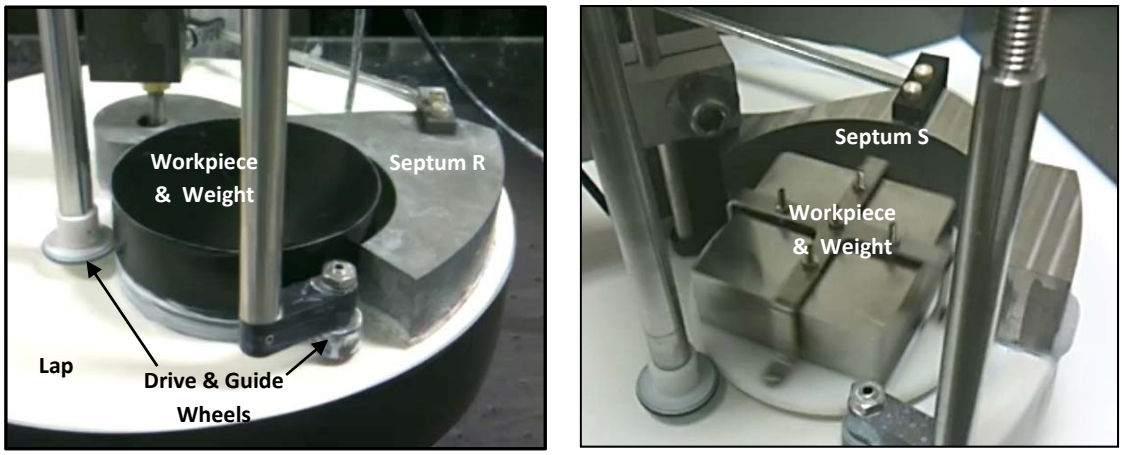

Figure 2.

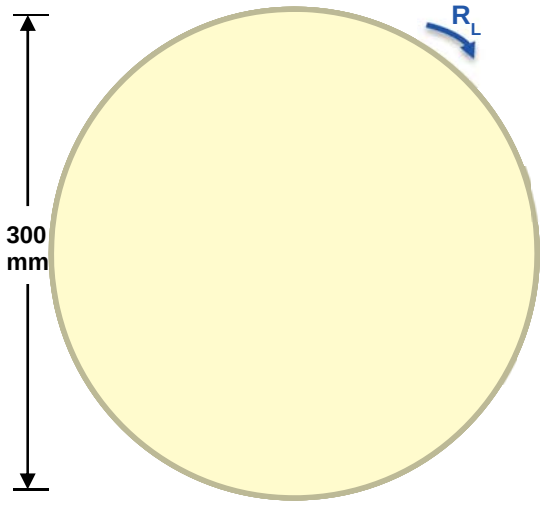

Figure 3.

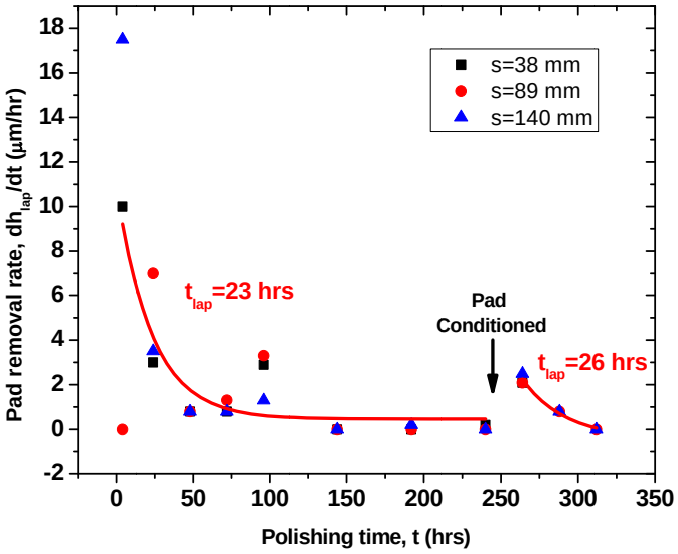

Figure 4.

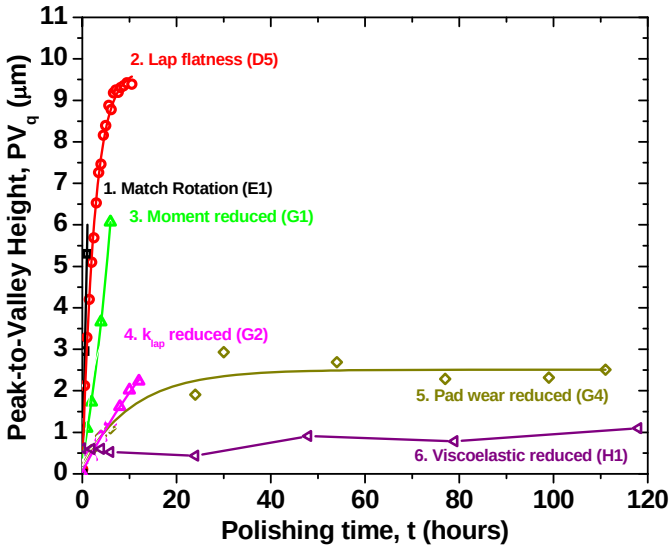
Peak-to-Valley Height, PV_q (μm)
Polishing time, t (hours)
2. Lap flatness (D5)
1. Match Rotation (E1)
3. Moment reduced (G1)
4. k_{lap} reduced (G2)
5. Pad wear reduced (G4)
6. Viscoelastic reduced (H1)
0
1
2
3
4
5
6
7
8
9
10
11
0
20
40
60
80
100
120

Figure 5.

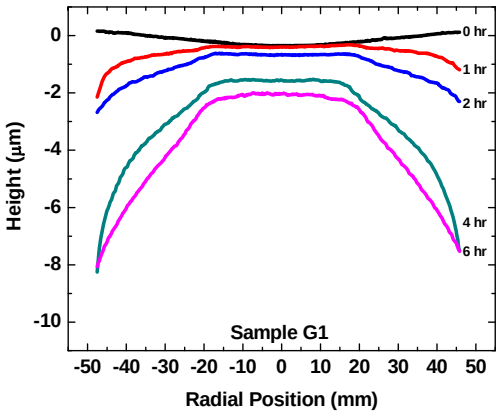
0
-2
-4
-6
-8
-10
Height (µm)
0 hr
1 hr
2 hr
4 hr
6 hr
Sample G1
-50 -40 -30 -20 -10 0 10 20 30 40 50
Radial Position (mm)

(a)

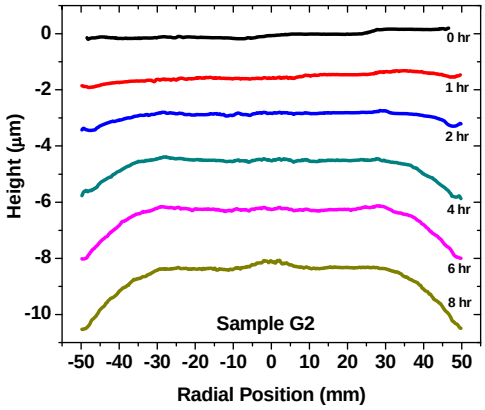
0
-2
-4
-6
-8
-10
Height (µm)
0 hr
1 hr
2 hr
4 hr
6 hr
8 hr
Sample G2
-50 -40 -30 -20 -10 0 10 20 30 40 50
Radial Position (mm)

(b)

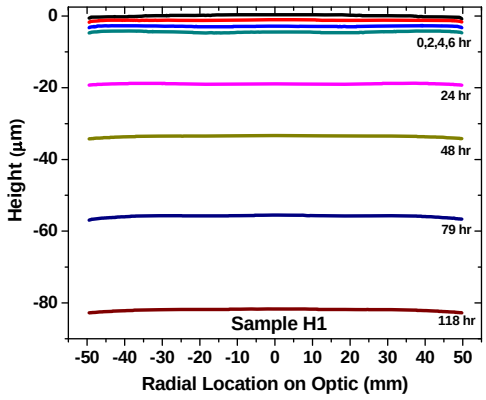
0
-20
-40
-60
-80
Height (µm)
0,2,4,6 hr
24 hr
48 hr
79 hr
118 hr
Sample H1
-50 -40 -30 -20 -10 0 10 20 30 40 50
Radial Location on Optic (mm)

(c)

Figure 6.

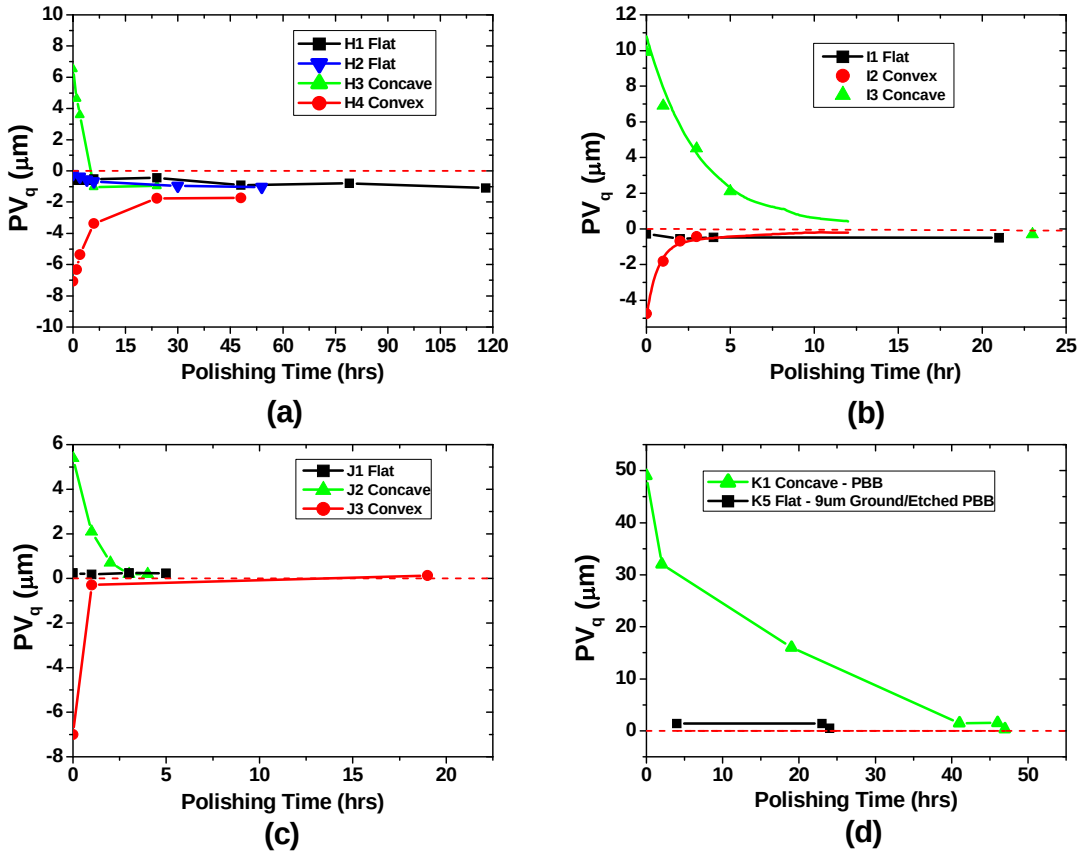
H1 Flat
H2 Flat
H3 Concave
H4 Convex
PV$_q$ (µm)
Polishing Time (hrs)
(a)
I1 Flat
I2 Convex
I3 Concave
PV$_q$ (µm)
Polishing Time (hr)
(b)
J1 Flat
J2 Concave
J3 Convex
PV$_q$ (µm)
Polishing Time (hrs)
(c)
K1 Concave - PBB
K5 Flat - 9um Ground/Etched PBB
PV$_q$ (µm)
Polishing Time (hrs)
(d)

Figure 7.

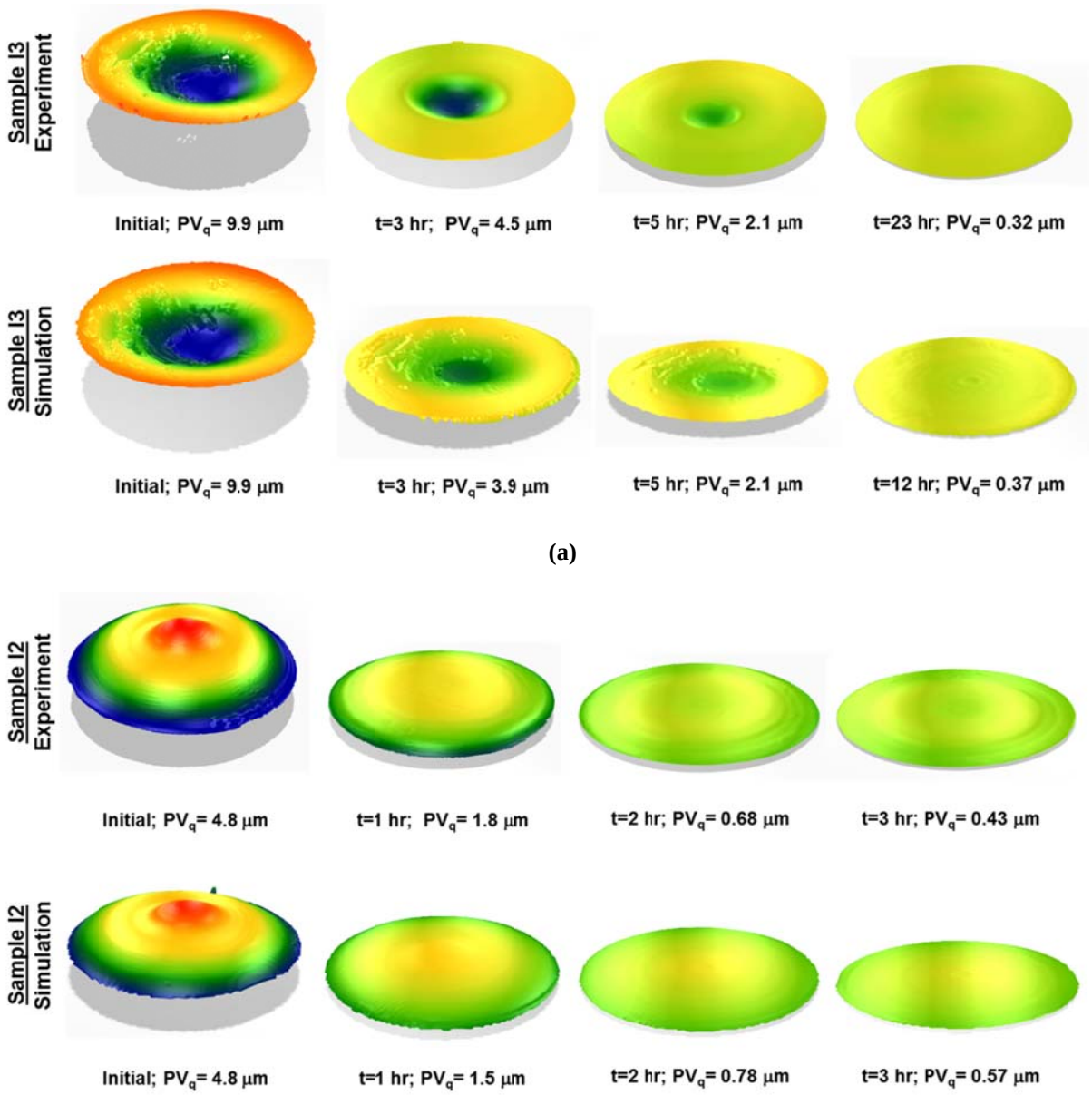
Sample I3
Experiment
Initial; PVq= 9.9 μm
t=3 hr; PVq= 4.5 μm
t=5 hr; PVq= 2.1 μm
t=23 hr; PVq= 0.32 μm
Sample I3
Simulation
Initial; PVq= 9.9 μm
t=3 hr; PVq= 3.9 μm
t=5 hr; PVq= 2.1 μm
t=12 hr; PVq= 0.37 μm
(a)
Sample I2
Experiment
Initial; PVq= 4.8 μm
t=1 hr; PVq= 1.8 μm
t=2 hr; PVq= 0.68 μm
t=3 hr; PVq= 0.43 μm
Sample I2
Simulation
Initial; PVq= 4.8 μm
t=1 hr; PVq= 1.5 μm
t=2 hr; PVq= 0.78 μm
t=3 hr; PVq= 0.57 μm
(b)

Figure 8.

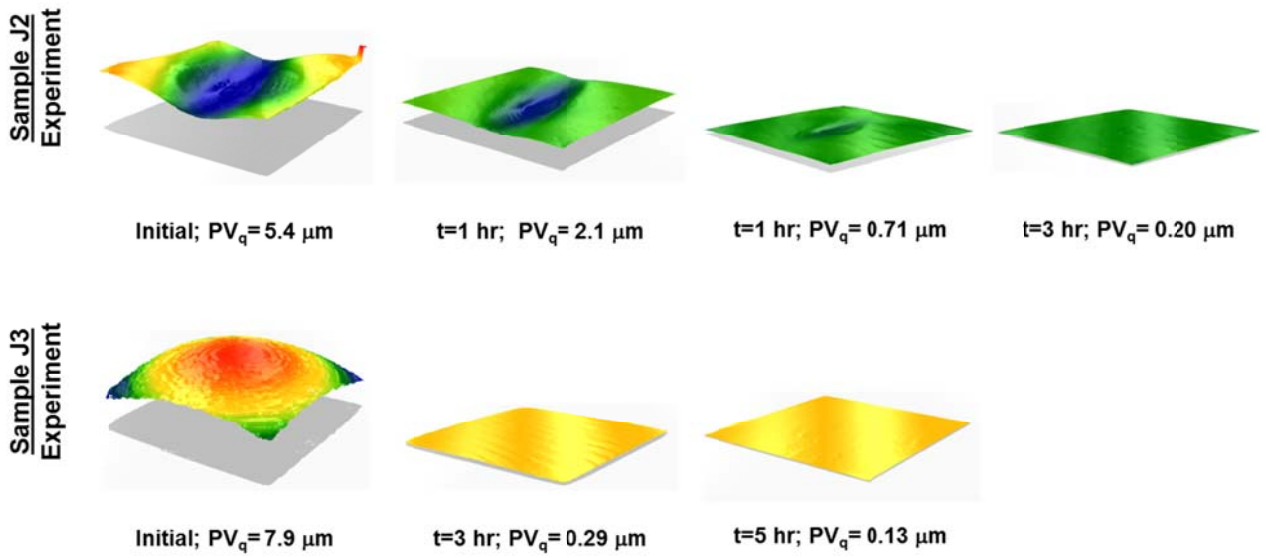
Sample J2
Experiment
Initial; PVq= 5.4 μm
t=1 hr; PVq= 2.1 μm
t=1 hr; PVq= 0.71 μm
t=3 hr; PVq= 0.20 μm
Sample J3
Experiment
Initial; PVq= 7.9 μm
t=3 hr; PVq= 0.29 μm
t=5 hr; PVq= 0.13 μm

Figure 9.

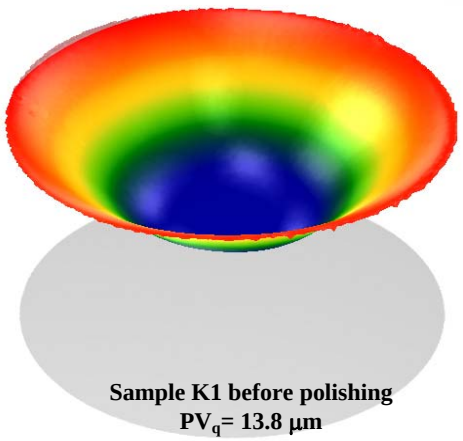

Sample K1 before polishing
PV_q= 13.8 µm
(a)

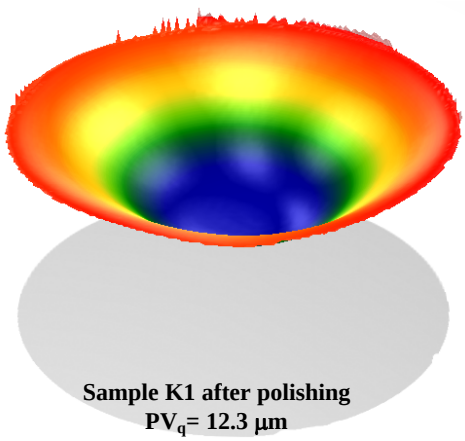

Sample K1 after polishing
PV_q= 12.3 µm
(b)

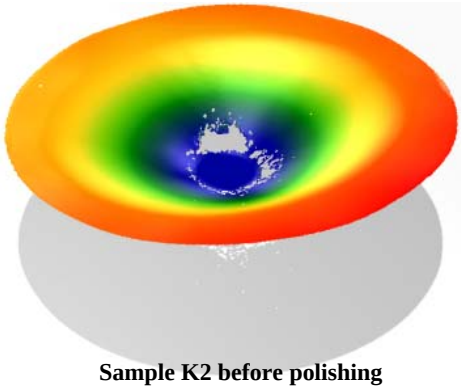

Sample K2 before polishing
PV_q= 22.5 µm
(c)

Sample K2 after polishing
PV_q= 0.91 µm
(d)

Figure 10.

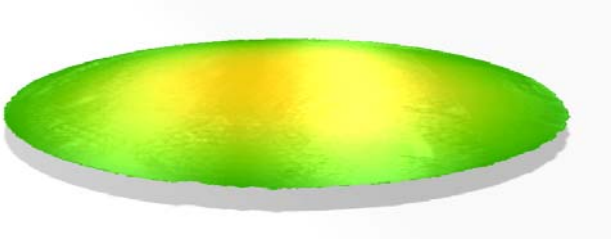

Sample K3 before 9 μm grind
PV_q= -1.14 μm
(a)

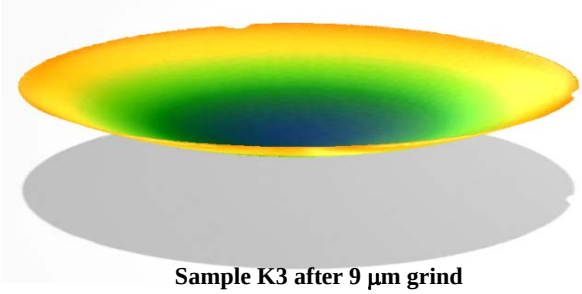

Sample K3 after 9 μm grind
PV_q= 3.65 μm
(b)

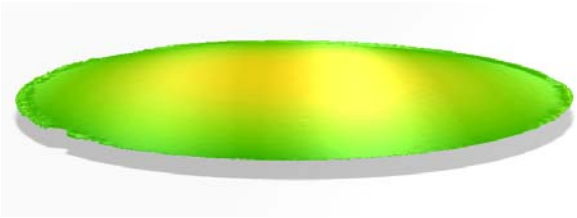

Sample K4 before 30 μm grind
PV_q= -1.35 μm
(c)

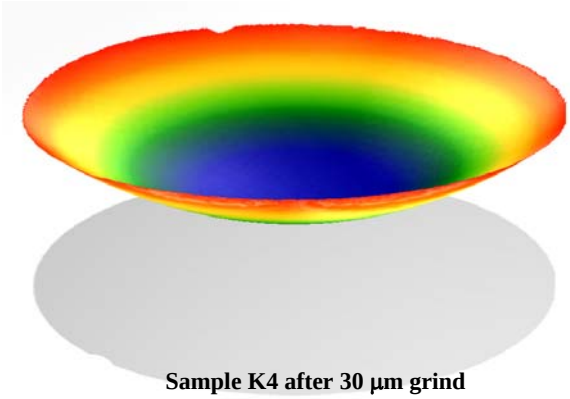

Sample K4 after 30 μm grind
PV_q= 7.70 μm
(d)

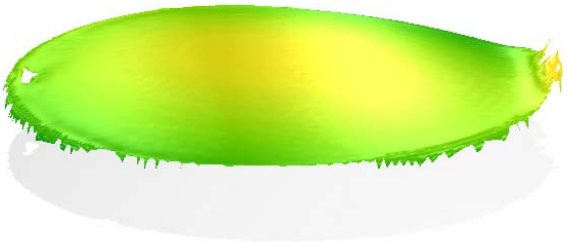

Sample K5 after 9 μm grind & etch
PV_q= -1.65 μm
(e)

Figure 11.

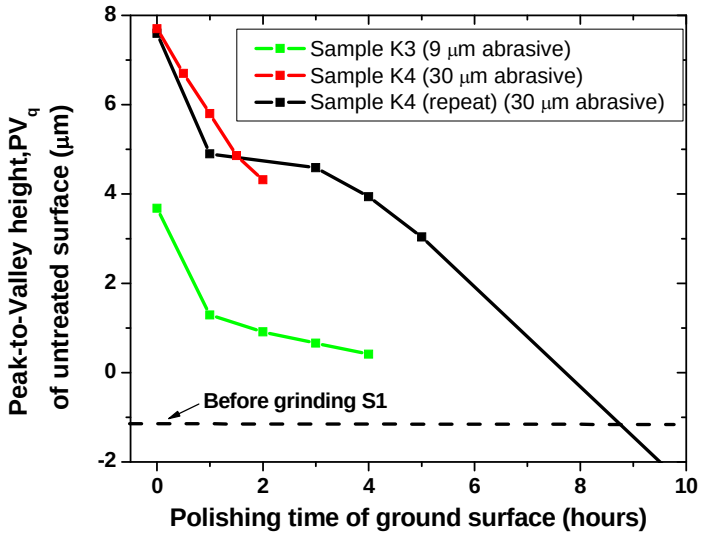
Sample K3 (9 μm abrasive)
Sample K4 (30 μm abrasive)
Sample K4 (repeat) (30 μm abrasive)
Before grinding S1
Peak-to-Valley height,PV$_q$ of untreated surface (μm)
Polishing time of ground surface (hours)
8
6
4
2
0
-2
0
2
4
6
8
10

Figure 12.

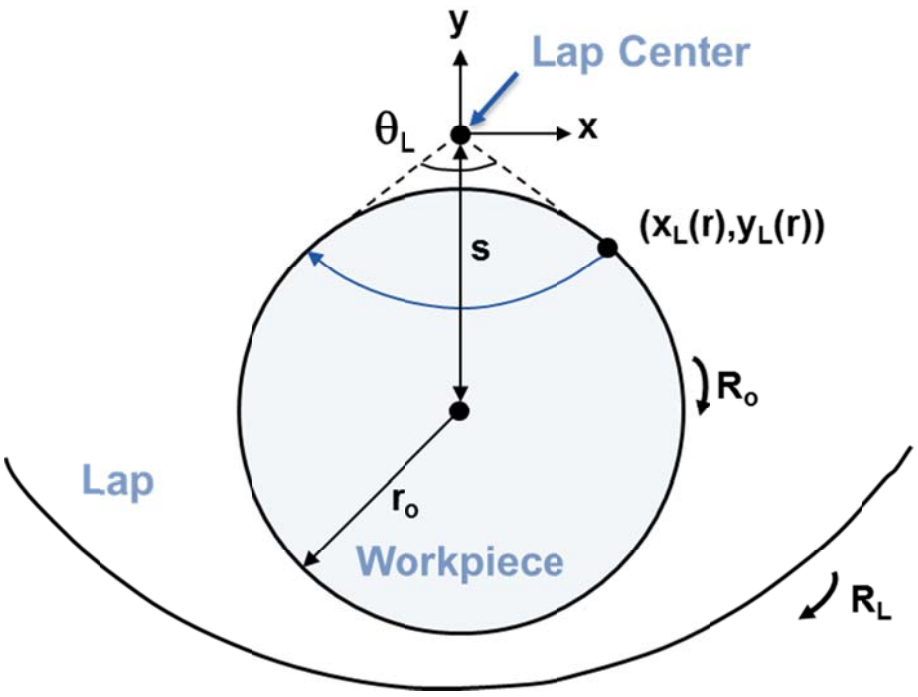

Figure 13.

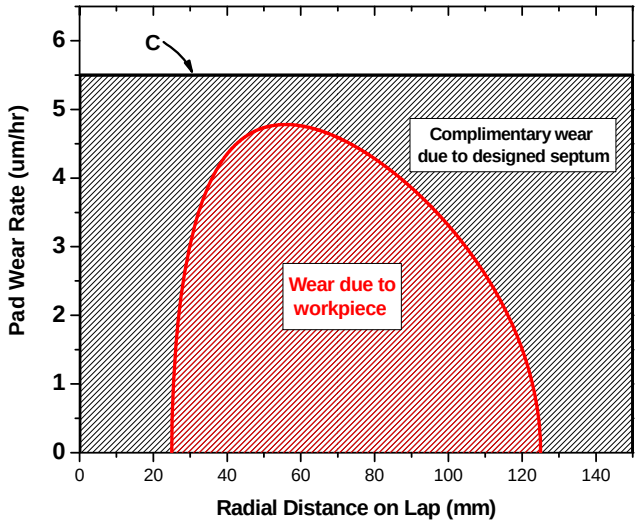
C
Complimentary wear
due to designed septum
Wear due to
workpiece
Pad Wear Rate (um/hr)
Radial Distance on Lap (mm)
0
1
2
3
4
5
6
0
20
40
60
80
100
120
140

(a)

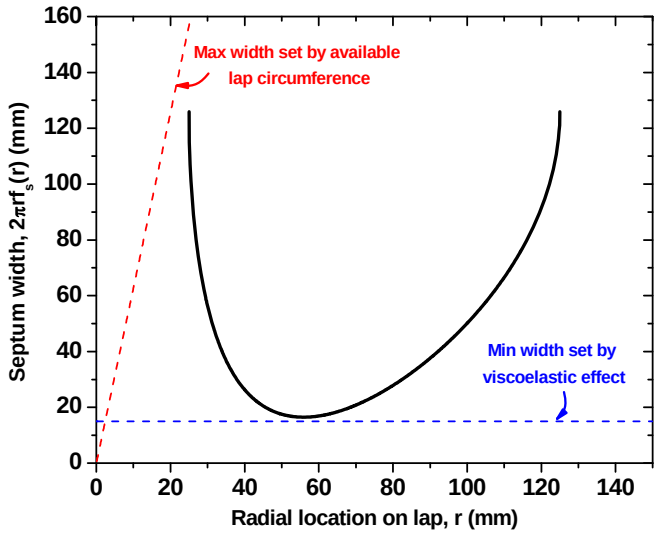
Max width set by available
lap circumference
Min width set by
viscoelastic effect
Septum width, 2πrf_s(r) (mm)
Radial location on lap, r (mm)
0
20
40
60
80
100
120
140
160

(b)

Figure 14.

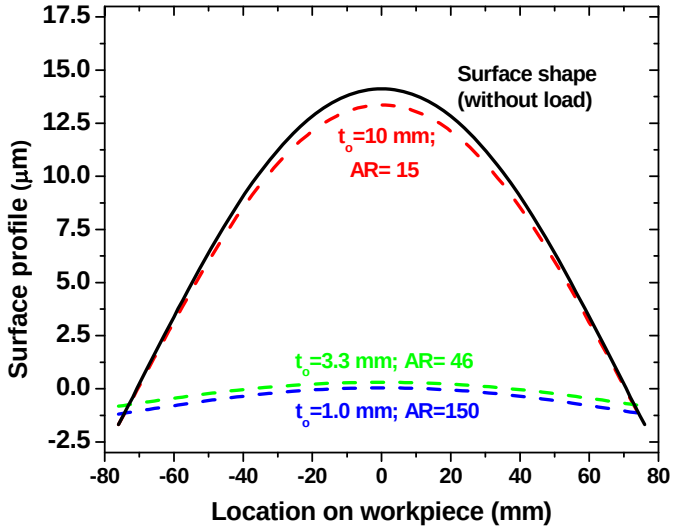
Surface shape
(without load)
t_o=10 mm;
AR= 15
t_o=3.3 mm; AR= 46
t_o=1.0 mm; AR=150
Surface profile (μm)
Location on workpiece (mm)
17.5
15.0
12.5
10.0
7.5
5.0
2.5
0.0
-2.5
-80
-60
-40
-20
0
20
40
60
80

Figure 15.